AMERICAN JOURNAL OF DIAGNOSTIC IMAGING
2024; 10(4): 77-81.
10.5455/ajdi.20240322021817

WisdomGale

CASE REPORT

Open Access

Extraskeletal Ewing sarcoma—A deceptive entity on imaging

Geetha Ganesan, Thiagarajan Veerappan, Kalpana Sivalingam
Barnard Institute of Radiology, Madras Medical College, Chennai, India

ABSTRACT

Background: Ewing sarcoma arising from soft tissue is referred to as an extraskeletal ewing sarcoma (EES). It is a rare tumor that primarily affects young people and has an aggressive course with a high recurrence rate. Imaging findings of EES tumors are generally non-specific, with some variation based on location and the tissues involved.

Case summary: We present two rare cases of EES in adolescent females: one from the right kidney masquerading as renal cell carcinoma (case 1), and the other one primarily arising from the left chest wall (case 2).

Conclusion: EES, albeit rare, should be considered in patients with large, heterogeneous soft tissue masses. Radiologists should be aware of this deceptive entity because, despite its non-specific appearance, imaging can assist in determining tumor extent, surrounding infiltration, distant metastasis identification, surgical feasibility, and thus the best treatment options.

ARTICLE HISTORY

Received March 22, 2024
Accepted September 19, 2024
Published September 27, 2024

KEYWORDS

Extra-skeletal Ewing Sarcoma (EES); renal cell carcinoma; chest wall lesion

Introduction

Extraskeletal ewing sarcoma (EES) is a rare, malignant soft tissue neoplasm that belongs to the ewing sarcoma family of tumors (ESFTs). This family consists of malignant small round cell tumors, including classical ES of bone (ESB), EES, Askin tumor (thoracopulmonary EES), and primitive neuroectodermal tumor (PNET) [1]. Though previously thought to be distinct neoplasms, these tumors now appear to share a common mesenchymal stem cell origin, with the distinction being based on the tumors' varying degrees of cellular differentiation and anatomical location [2]. EES is less common than its intraosseous counterpart, accounting for only 15%–20% and primarily affecting adolescents and young adults aged 10 to 30 years old with an aggressive course [3]. We present two rare cases of EES in adolescent females: one from the right kidney masquerading as renal cell carcinoma (patient 1), and the other one primarily arising from the left chest wall (patient 2).

Case reports

Case 1. An 18-year-old girl presented to our hospital with complaints of fever, cough, and breathlessness for the past two weeks. The patient also experienced significant weight loss and loss of appetite but had no prior respiratory illnesses or tuberculosis. The patient was referred to us for chest imaging. A frontal chest radiograph revealed numerous bilateral lung nodules, as well as obliteration of the right costophrenic and cardiophrenic angles (Fig. 1).

A contrast-enhanced computerized tomography (CECT) of the chest was then performed, revealing multiple heterogeneously enhanced nodules of varying sizes throughout both lungs. The largest nodule measured up to 4.6 cm in the right lower lobe. A large right-sided pleural effusion was associated with compressive atelectasis in the underlying right lung, primarily affecting the right lower lobe, which had nearly collapsed. Nodularity was also found on both pleural surfaces, raising concerns about pleural metastatic disease. Multiple enlarged mediastinal and internal mammary lymph nodes were also observed (Fig. 2a and b). The adrenal glands were normal. Surprisingly, the extended field of view (FOV) revealed a hypo-dense, heterogeneously enhancing mass measuring 9.5 × 6.8 cm in the right kidney's lower pole. No areas of internal calcification or fat were found. There was also a filling defect in the right main renal vein, which extended up to the inferior vena cava (Fig. 3a and b).

Contact Geetha Ganesan ✉ drgeethamdrd@gmail.com Barnard Institute of Radiology, Madras Medical College, Chennai, India.

© The Author(s) 2024. Open Access. This article is licensed under a Creative Commons Attribution 4.0 International License (CC BY).
http://creativecommons.org/licenses/by/4.0/.

Later, the patient had an ultrasound examination of both kidneys, which showed an ill-defined iso- to a slightly hypoechoic lesion in the lower pole of the right kidney (Fig. 4a). Color Doppler imaging revealed minimal vascularity in the mass (Fig. 4b) and none in the right main renal vein. The left kidney was normal.

The patient was then referred for a positron emission tomography (PET) scan, which demonstrated increased metabolic activity in the lower pole of the right kidney as well as multiple pulmonary and pleural lesions (Fig. 5a and b). The imaging results indicated a provisional diagnosis of a right renal primary tumor with renal vein tumor thrombosis and multiple pleural, pulmonary, mediastinal, and internal mammary lymph nodal metastases.

The kidney mass was then biopsied under ultrasound guidance. Light microscopy revealed sheets of small round blue cells with scant cytoplasm and dark nuclei, indicating a high nucleo-cytoplasmic ratio. Immunohistochemistry (IHC) showed that the tumor cells expressed CD99, and FLI1 (Fig. 6a–c). The pathology report indicated EES of the kidney. The patient was scheduled for combination chemotherapy due to her metastatic status at the time of presentation. Unfortunately, the patient died from her illness before any treatment could be administered.

Case 2. A 12-year-old girl came to our hospital complaining of breathlessness, cough, dysphagia, and

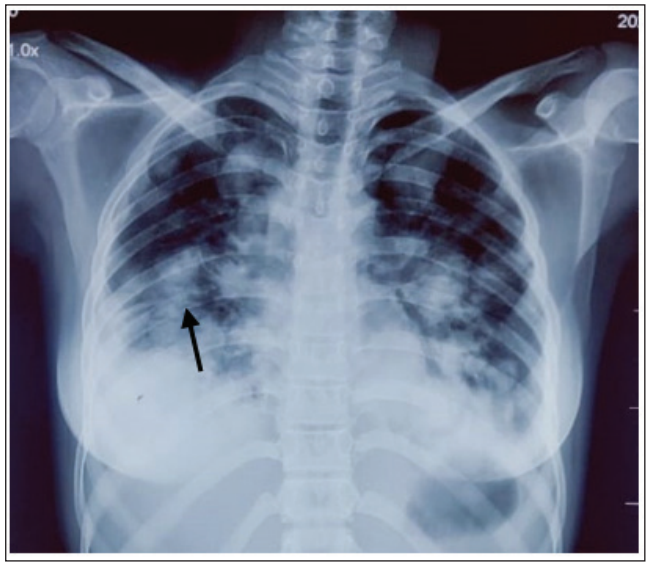


Figure 1. Frontal chest radiograph (CXR) shows numerous bilateral lung nodules (black arrow) with obliterated right costophrenic and cardiophrenic angles.

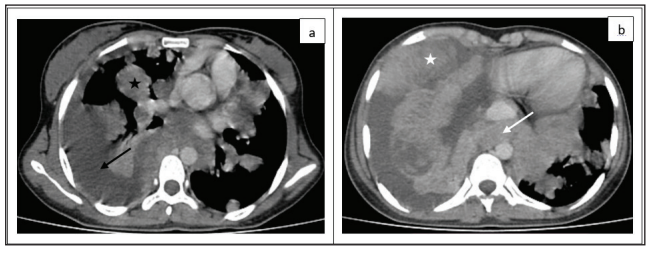


Figure 2. (a, b) Axial contrast-enhanced computed tomography images show multiple lung nodules (black star), pleural nodules (white star), mediastinal lymph nodes (white arrow) and right pleural effusion (black arrow).

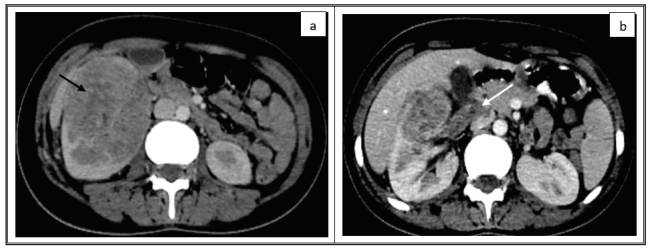


Figure 3. (a) Axial contrast-enhanced computed tomography extended FOV images show heterogeneously enhancing mass in lower pole of right kidney (black arrow). (b) Filling defect noted in right renal vein extending upto IVC reflecting tumor thrombus (white arrow).

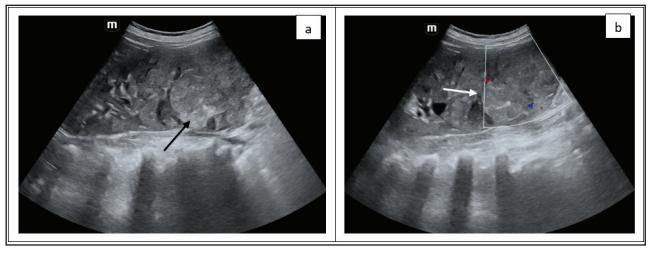


Figure 4. (a) Sagittal Gray Scale Sonography image of the right kidney shows an ill-defined isoechoic mass (black arrow) in the lower pole. (b) Colour Doppler image shows minimal vascularity within the mass lesion (white arrow).

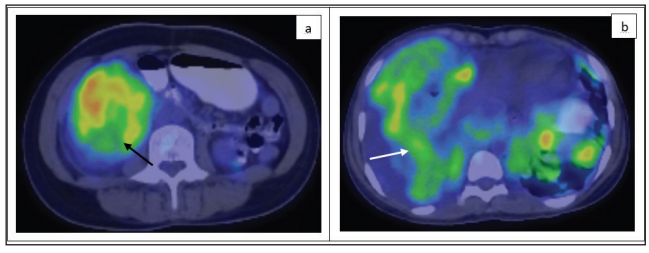


Figure 5. (a, b) Axial positron emission tomography images show increased metabolic activity in the lower pole of right kidney (black arrow) and in multiple pulmonary and pleural lesions (white arrow).

left-sided chest pain for the past month. She also lost a lot of weight but had no major medical history. The patient was tachypneic at the time of presentation, so a plain X-ray of the chest was taken, revealing a complete opacification of the left hemithorax with cut-off of the left main bronchus and mediastinal shift to the opposite side (Fig. 7).

A CECT of the chest revealed a large irregularly lobulated soft tissue density mass measuring approximately 14.6 × 15.3 × 19.2 cm that occupied the entire left hemithorax and was most likely originating from the left chest wall (Fig. 8a–c). The mass was compressing the carina, the left main pulmonary artery, and the lower part of the esophagus down to the esophagogastric junction, resulting in the passive, near-complete collapse of the left lung. The mass had a heterogeneous texture and an internal necrotic component with no intratumoral calcifications. It also caused erosion of the inner aspect of the adjacent left seventh rib, resulting in a lamellated periosteal reaction (Fig. 9). The right lung was normal. Based on the imaging findings, germ cell tumors, lymphoma, EES, and rhabdomyosarcoma were considered as the differentials.

The patient consented to an emergency posterolateral thoracotomy, and the mass was debulked (Fig. 10). Histopathology showed sheets of small round blue cells with dark nuclei and scant cytoplasm (Fig. 11), whereas immunohistochemistry revealed strong membrane positivity with CD-99 and nuclear positivity with NKX2.2 and FLI1, respectively (Fig. 12a–c). These observations led to a confirmatory diagnosis of Askin tumor

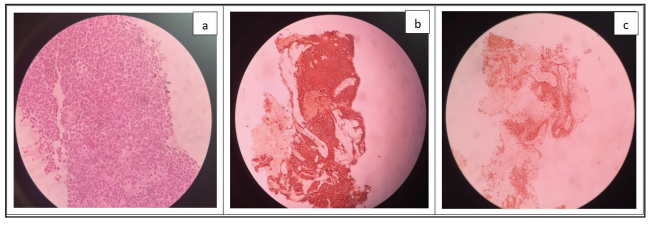


Figure 6. (a) High power view shows hematoxylin and eosin stained tumor cells arranged in sheets with hyperchromatic nuclei and scant cytoplasm. (b, c) Low power view shows tumor cells are positive for CD99 and FLI1 respectively.

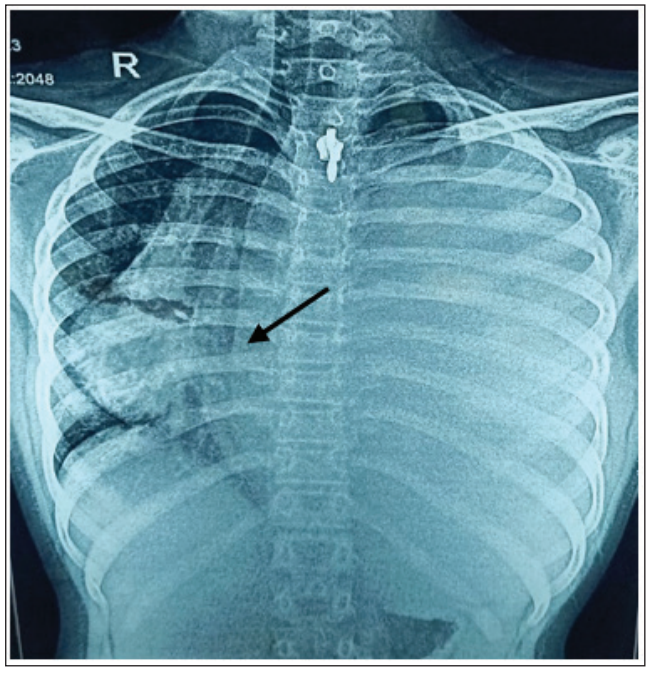


Figure 7. Frontal CXR shows complete opacification of the left hemithorax with resultant mediastinal shift to the right and cut-off of the left main bronchus (black arrow).

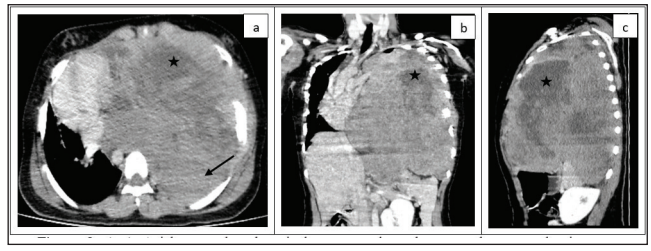


Figure 8. (a–c) Axial, coronal and sagittal contrast-enhanced computed tomography images demonstrate left chest wall mass which enhance heterogeneously (black arrow) with patchy hypodense areas suggestive of necrosis (star). There is atelectasis of the left lung and mediastinal shift to the right.

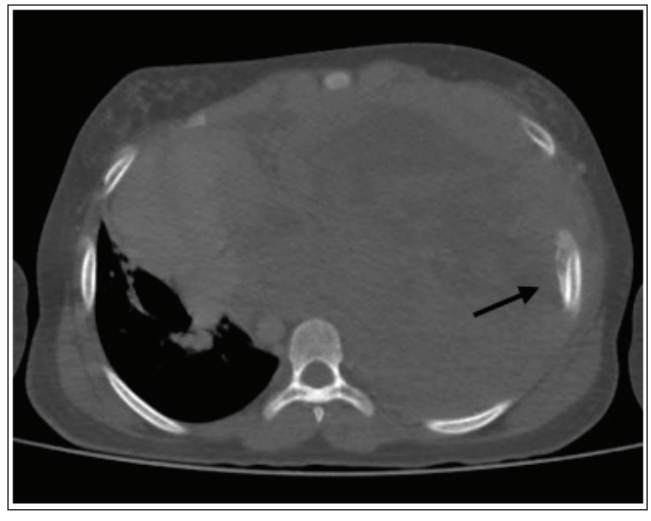


Figure 9. Axial computed tomography of the chest on bone window demonstrates the lamellated periosteal reaction of the left seventh rib (black arrow)

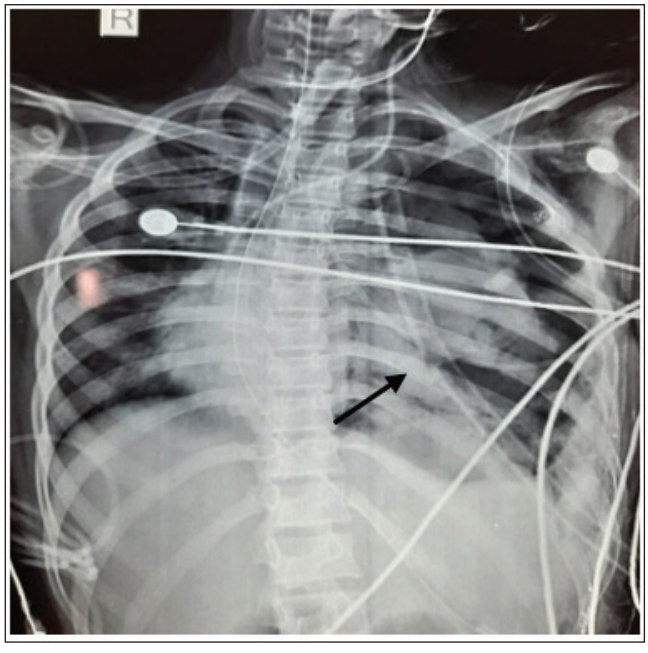


Figure 10. Post-operative frontal CXR shows reduction in the size of mass with re-expansion of the left lung and intercostal drainage (ICD) tube noted in situ. (Black arrow).

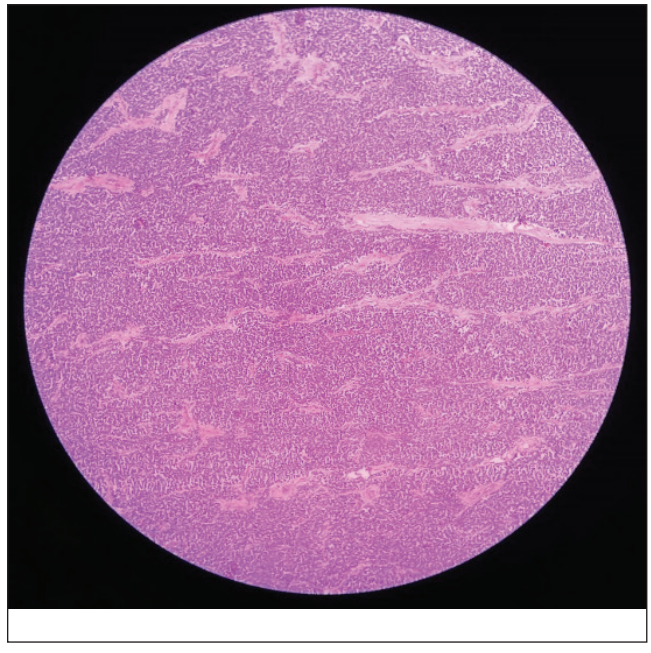


Figure 11. Low power view shows hematoxylin and eosin stained tumor cells arranged in sheets with hyperchromatic nuclei and scant cytoplasm.

(thoracopulmonary EES), and the patient is now on a systemic chemotherapy regimen with alternating programs of vincristine, doxorubicin, cyclophosphamide (VDC) and ifosfamide, and etoposide (IE).

Discussion

ESFT is a recently proposed and increasingly accepted single biologic entity that combines ESB, EES, Askin tumor (thoracopulmonary EES), and PNET. ESFTs are malignant small round cell tumors with varying degrees of neuroectodermal differentiation. The most distinguishing feature is that these lesions possess the same karyotype abnormality: a non-random reciprocal translocation of chromosomes 11 and 22 (t[11;22][q24;q12]). The 22q12 locus codes for EWS, while the 11q24 site codes for FL1, resulting in the EWS-FL1 fusion transcript, which occurs in 85%–95% of cases [4].

Pediatric patients with ES usually have skeletal ES, whereas adults have a higher proportion of EES than children. The EES is simply an ewing sarcoma that originates in the soft tissues. It typically manifests as a large, rapidly growing solitary mass that can appear anywhere in the body. Primary EES tends to affect the extremities (particularly the lower extremities), soft tissues of the trunk, like the paravertebral and intercostal regions, the head and

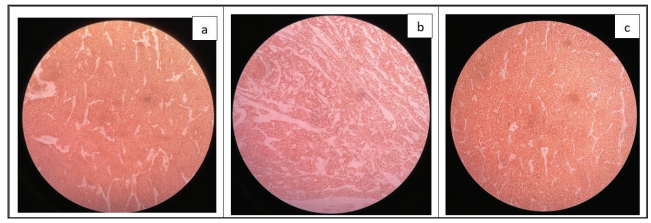


Figure 12. (a–c). Low power views show tumor cells are exhibiting membrane positivity for CD99, and nuclear positivity for NKX2.2, and FLI1 respectively.

neck, the pelvis, the peritoneum, and the retroperitoneum [5]. The lung is a rare organ with primary EES involvement, but it is the most common site for metastasis [6].

EES's primary symptoms are non-specific and include pain, fever, anorexia, and weight loss. Thus, the primary symptoms are heavily influenced by the location of the primary tumor and metastasis [7]. Due to the rarity of EES, diagnosis and treatment can be challenging. Although the imaging presentation of EES is deceptive due to the presence of other equivalent tumors with similar imaging characteristics, imaging modalities are used solely to make the initial diagnosis. However, the final diagnosis is primarily based on the histopathology and immunohistochemistry of soft tissue samples.

In ultrasound, EES lesions are most frequently hypoechoic with few anechoic areas and show

intratumor flow signals in a Doppler study [8]. The most common CECT findings for EES are a heterogeneously enhancing mass with an occasional central, non-enhancing area reflecting hemorrhage or necrosis [9]. Approximately 25% of cases have faint amorphous calcifications. EES usually do not have any osseous components, but they can cause secondary bone surface involvement, like cortical erosion or periosteal reaction, in up to 40% of cases [6].

On MRI (magnetic resonance imaging), the EES lesion displays low signal intensity on T1-weighted sequences and high signal intensity on T2-weighted images, with heterogenous post-contrast enhancement [10]. Approximately 15%–46% of patients have gross metastatic disease at the time of presentation, with the lung being the most common location of metastasis. PET-CT is extremely useful in detecting distant metastases. Once the diagnosis is confirmed, the most effective treatment for EES is a combination of surgery, neoadjuvant and postoperative chemotherapy, radiotherapy, and targeted drug therapy.

Conclusion

EES, albeit rare, should be considered in patients with large, heterogeneous soft tissue masses. Radiologists should be aware of this deceptive entity because, despite its non-specific appearance, imaging can assist in determining tumor extent, surrounding infiltration, distant metastasis identification, surgical feasibility, and thus, the best treatment options.

Funding

None.

Conflict of interest

None declared.

References

1. Nasri S, Aqamour R, Haddar L, Guerrouj I, Haddar K, Aichouni N, et al. Extraskeletal Ewing sarcoma: a case report. Radiol Case Rep 2022 Dec; 17(12):4809–13.
2. Javery O, Krajewski K, O'Regan K, Kis B, Giardino A, Jagannathan J, et al. A to Z of Extraskeletal Ewing sarcoma family of tumors in adults: imaging features of primary disease, metastatic patterns, and treatment responses. Am J Roentgenol 2011 Dec; 197(6):W1015–22.
3. El-Essawy MT. Extraskeletal Ewing's sarcoma. Saudi Med J Int 2009; 30(6):840. Available via https://pubmed.ncbi.nlm.nih.gov/19526172/
4. Wei CK, Nadarajan C. Retroperitoneal Extraskeletal Ewing's Sarcoma in adult. Borneo J Med Sci (BJMS) Int 2023; 17(1):26–31. Available from: https://jurcon.ums.edu.my/ojums/index.php/bjms/article/view/3879
5. Avcu S, Akdeniz H, Bora A, Arslan H, Ünal Ö. Primary Extraskeletal Ewing sarcoma originating from chest wall in a Child. Eur J Gen Med 2010; 7(1):101–3; doi:https://doi.org/10.29333/ejgm/82828
6. Wright A, Desai M, Bolan CW, Badawy M, Guccione J, Rao Korivi B, et al. Extraskeletal Ewing sarcoma from head to toe: multimodality imaging review. Radiographics. 2022 Jul 1; 42(4):1145–60.
7. Abboud A, Masrouha K, Saliba M, Haidar R, Saab R, Khoury N, et al. Extraskeletal Ewing sarcoma: diagnosis, management and prognosis (Review). Oncol Lett 2021 Mar 4; 21(5).
8. Choudhury AR, Jain SG, Reghunath A, Ghasi RG, Kaur N, Kolte S. Primary Ewing's sarcoma of the kidney: a rare masquerader of renal cell carcinoma on imaging. Egyptian J Radiol Nuclear Med 2022 Feb 23; 53(1):53.
9. Mathew D, Prince DN, Mahomed N. Extra-skeletal Ewing Sarcoma of the chest wall in a child. South Afr J Radiol 2019 Jun 27; 23(1):1.
10. Alexander A, Hunter K, Rubin M, Bhat AP. Extraosseous Ewing's Sarcoma: pictorial review of imaging findings, differential diagnosis, and pathologic correlation. Indian J Radiol Imag Int 2021 May 31; 31:203. Available from: https://www.ncbi.nlm.nih.gov/pmc/articles/PMC8299506/